# A Bioprinted *in vitro* Model for Osteoblast to Osteocyte Transformation by Changing Mechanical Properties of the ECM

*Bryan E.J. Lee [1], ‡, Alireza Shahin-Shamsabadi [1], ‡, Michael K. Wong [4], Sandeep Raha [4], [5], P Ravi Selvaganapathy [1],[2],*, Kathryn Grandfield [1],[3],**

[1]School of Biomedical Engineering, McMaster University, Canada

[2]Department of Mechanical Engineering, McMaster University, Canada

[3]Department of Material Science and Engineering, McMaster University, Canada

[4]Graduate Program of Medical Science, McMaster University, Hamilton, Ontario, Canada.

[5]Department of Pediatrics, McMaster University, Hamilton, Ontario, Canada.

Keywords: Bioprinting; *In vitro* model; Bone; Osteoblast; Osteocyte

Osteocytes are key contributors to bone remodeling. During the remodeling process, trapped osteoblasts undergo a phenotypic change to become osteocytes. The specific mechanisms by which osteocytes work are still debatable and models that exist to study them are sparse. This work presents an *in vitro*, bioprinted model based on the previously developed technique, ExCeL, in which we print and immediately crosslink a cell-embedded hydrogel using paper as a crosslinker-storing substrate. This process mimics the phenotypical change of osteoblast to osteocyte by altering the mechanical properties of the hydrogel. By printing Saos-2, osteosarcoma cells, embedded in alginate hydrogel with differing mechanical properties, we were able to change their morphology, protein and gene expression from osteoblast-like to osteocyte-like. The stiffer gel was 30 times stiffer and resulted in significantly smaller cells with reduced alkaline phosphatase activity and expression of osteoblast-marker genes such as MMP9 and TIMP2. There was no change in viability between cells despite encapsulation in gels with different mechanical properties. Our results show that the phenomenon of osteoblasts becoming encapsulated during the bone remodeling process can be replicated using the ExCeL bioprinting technique. This model has potential for studying how osteocytes can interact with external mechanical stimuli or drugs.

## 1. Introduction

Bone is a dynamic, hierarchical material that actively remodels itself in response to mechanical signals. One of the major constituents of the bone remodeling process are osteocytes, which come from osteoblasts that were entrapped during the bone remodeling [1], [2]. During the remodeling process, osteoblasts are slowly buried by bone matrix which is a combination of collagenous fibers and mineral deposits, otherwise known as osteoid. Over time this osteoid becomes mineralized leading to the formation of new bone tissue with embedded osteoblasts

which have now been differentiated into osteocytes. The expression of many proteins differs greatly between osteoblasts and osteocytes despite their shared lineage [3], [4]. One of the primary characteristics of osteocytes is that they translate external mechanical cues into biochemical actions which fuels the bone remodeling process, a process termed mechanotransduction [5]. Despite this important role in bone biology, there is a lack of available models or cell lines for *in vitro* studies of osteocytes role in bone remodeling or their response to stimuli. This is compounded by the fact that most *in vitro* systems are two-dimensional (2D) in nature and incapable of entrapping osteocytes. 2D culture systems are dominant and have been used extensively but often do not accurately represent the in vivo response [6]. This is predominantly due to their dimensional limitations and lack of environmental cues that cells would otherwise receive in the physiological environment such as mechanical properties of the extracellular matrix (ECM), nutrient and oxygen gradients, and inter-cellular and cell-matrix interactions [7], [8]. Different 3D systems have been developed that yield more accurate responses similar to natural tissues by recapitulating some of these features [9]. Compared to 2D cell culture systems, these 3D models can maintain the phenotype of cells [10] by controlling the polarity of cell-cell and cell-matrix contacts [11], [12], as well as mechanical properties of their environment [11], [12] and transport characteristics of important soluble growth factors [13].

The MLO-Y4 mouse cell line has been most commonly used to study osteocyte behavior with success but they are primarily utilized in 2D *in vitro* culture methods [14], [15]. Other researchers have created a three-dimensional (3D) model of osteocytes by embedding human osteoblasts in a mineral matrix comprised of biphasic calcium phosphate similar in composition to that of natural bone but this work has not considered the organic phase [16]. However, the specific mechanical entrapment required to initiate phenotypical changes of osteoblasts to

osteocytes has yet to be determined. Many studies involving 3D models for bone or osteocyte-behavior do not consider the specific mechanical properties required to entrap and influence differentiation from osteoblast to osteocyte [16], [17]. For a 3D model to be accurate it should exhibit the architectural complexities of native tissue and bioprinting has emerged as a promising technique [18], [19] for this purpose. Bioprinting evolved from additive manufacturing methods to use soft materials like gels and extracellular matrices which could support growth of cells and formation of tissue-like constructs [20], [21]. Bioprinting has enabled researchers to manufacture complex structures and constructs with biomaterials containing extracellular matrices and cells [21], [22] and to reproduce biophysical and biochemical microenvironment in physiological or pathological conditions in a well-defined manner with high accuracy [18], [23], [24].

This work investigates how changes in mechanical properties of non-mineralized bone matrix can influence the osteoblast to osteocyte phenotype transformation in a 3D environment using a bioprinting based technique named Combing Extrusion printing on Cellulose scaffolds with Lamination (ExCeL).

## 2. Methods Summary

A 3D *in vitro* model was developed using the ExCeL bioprinting technique [25] to study effect of mechanical properties of ECM on osteoblast to osteocyte phenotype transformation. Figure 1 summarizes this process. First, two different calcium chloride solutions (0.1 M and 1 M) were printed, with printing speeds of 1000 and 2000 mm/sec respectively, on chromatography paper. The first condition is referred to further as the low calcium (Low-Ca) content paper, and the second the high calcium (High-Ca) content paper). The papers were allowed to dry overnight. Subsequently, two different concentrations of alginate (2 and 3 wt% in McCoy's culture medium) embedded with bone cells from the Saos-2 cell line were printed on each of them (2

wt% on Low-Ca (2L) and 3 wt% on High-Ca papers (3H)). Alginate as a material lends itself well to the ExCeL process, which allows for tuning of the gel stiffness, compared to collagen or gelatin [25]. Additionally, it is also the most commonly used hydrogel in bioprinting processes and has seen success printing with Saos-2 cells [39],[40]. These hydrogels crosslink immediately upon contact with the paper and reside on top of it thus giving it mechanical properties independent of the paper. The 300 μm tall cylinder shape, calculated from volume of printed hydrogel and covered area, was chosen such that the scaffold would be a homogeneous shape and thus prevent mass transfer induced gas or nutrient gradients which could alter the morphology or phenotype of the cells. It was assumed that 2L condition would yield lower stiffness compared to the 3H condition and hence cells would change to more osteocyte like phenotype in the 3H samples with higher stiffness. Other conditions were experimented with but did not generate sufficient differences in preliminary protein expression experiment to warrant further investigation (Supplementary Figure 1).

Mechanical properties of the two condition were evaluated and compared using a Microsquisher mechanical tester. Viability of the cells in these conditions was compared using Alamar blue assay (ABA) and live/dead staining kit. Total protein synthesized by cells in each condition, as well as amount of alkaline phosphatase activity, a biomarker of osteoblast cells, was studied using pierce BCA protein and alkaline phosphatase kits. Using Quantitative Reverse Transcription Polymerase Chain Reaction (qRT-PCR) several genes that are highly expressed in either osteoblasts or osteocytes were investigated to further study the phenotype change. SEM of these 3D printed samples was performed to compare morphology of cells in each of these conditions. Fluorescent microscopy of samples stained with DAPI and Nile Red was performed, and cell sizes were compared in different conditions.

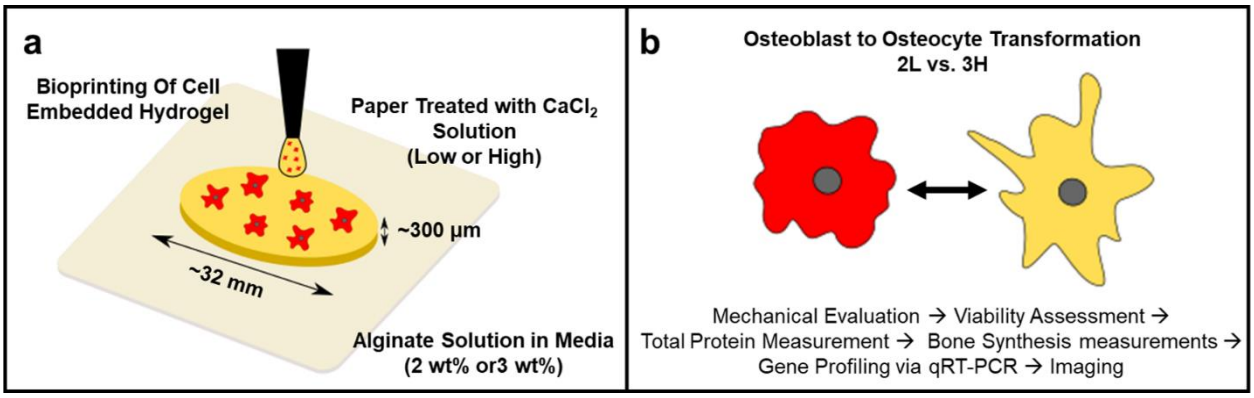


**Figure 1.** Design of experiment, a) Bioprinting procedure, b) Phenotype change confirmation through series of experiments. Using the ExCeL process, Saos-2 cells are encapsulated in an alginate hydrogel using different amounts of crosslinker and wt% to create scaffolds with differing stiffnesses. The encapsulated cells in these scaffolds are subsequently evaluated based on their phenotype.

## 3. Materials and Methods

### 3.1. Bioprinting Setup

Development of the 3D *in vitro* model was performed using the ExCeL process [26]. It starts by pretreating the paper (Whatman® cellulose chromatography papers, Grade 3 MMCHR) with the alginate crosslinker (calcium chloride solution, Sigma Aldrich). In order to create the required 3D structures, alginic acid sodium salt (Sigma-Aldrich) solutions were printed in concentric circles that are 1.5 mm apart with the printing speed of 500 mm/min and hydrogel flow rate of 0.5 mL/min to form a circle with diameter of 26 mm. Because of the presence of calcium (Ca) on paper, the hydrogel crosslinks rapidly upon touching the paper and maintains

the desired pattern. After printing is complete, samples were kept on the printing stage for 10 more minutes to allow complete crosslinking of the hydrogel and then they were transferred to a 6 well plate, where they were washed with PBS to remove excess amounts of Ca. Eventually samples were soaked in 2 mL culture medium that was changed every 2 days.

### 3.2. Mechanical testing

Mechanical properties of the printed structures were evaluated using a MicroSquisher machine (Cell Scale Biomaterials Testing, model). A 2×2 mm stainless steel platen connected to a 0.5 mm diameter cantilever was pressed towards the center part of the hydrogel at a defined rate (10% of the total thickness of the hydrogel per minute) in a displacement-controlled setup. Displacement of the platen was tracked by analyzing images taken by a camera while a load cell connected to the other end of cantilever measured the amount of force exerted by the hydrogel. The force-displacement data were then translated to stress-strain curves and the Young's modulus was defined as the slope of the initial linear range of the diagram. The ratio of Young's modulus of 3H to 2L was reported to compare difference between mechanical properties of the chosen conditions. Five samples were tested for each condition.

### 3.3. Viability

Saos-2 (ATCC®), osteosarcoma, cells were cultured in McCoy's 5A modified medium (Life Technologies Inc) with 15% fetal bovine serum (FBS) (Life Technologies Inc) and 1% penicillin/streptomycin (Life Technologies Inc). Cells were detached when confluent and mixed with alginate (2 or 3 wt% in McCoy's medium) before printing at a concentration of 2 x 106 cells/mL alginate solution.

Viability of the cells was assessed using a live/dead assay kit (Molecular Probes, Oregon, USA) where the concentration was 2 μM Calcein AM and 4 μM ethidium homodimer-1 for live

and dead respectively. Media was removed from wells following one day of the cells being embedded in the hydrogel matrix and the stain was added for 1 hour. Following incubation at 37oC, the samples were observed using an Olympus BX53F upright light microscope (Olympus, USA) using 475-485/485-536 nm (FITC) and 542-582/582-644 nm (TXRED) filters for the live and dead stains respectively. Samples were also examined for cell metabolism using an Alamar blue® (Life Technologies Inc.) assay following one day of incubation. Media was removed from the samples and replaced with a 5% Alamar blue® solution (in McCoy's 5A medium). Samples were incubated for 1 hour in the dark at 37oC before measuring fluorescence using an Infinite® M200 (Tecan, Männedorf, Switzerland) at 540-580 nm (excitation-emission).

In order to measure the effect of chosen conditions on cell morphology, 7-day old samples were fixed and stained using Nile Red and DAPI. First 10 µL of Nile Red stock solution (10 mg/mL in acetone) was diluted in 10 mL PBS and 3 mL of this solution was added to each sample followed by 10 min incubation. Then samples were counterstained with 3 mL of working solution of DAPI that was prepared by dissolving 2.9 µL of its stock solution (5 mg/mL in PBS) in 10 mL PBS. Incubation time for this step was also 10 min. Finally, samples were washed with PBS and imaged using an upright microscope and 10X magnification.

### 3.4. Protein Assays

Following 4, 7 and 14 days of incubation, hydrogel samples were rinsed with PBS before being dissolved using 3 mL of sodium citrate (0.1 M) on a shaker.2 mL of the suspended cell solution was aliquoted for PCR while the remaining 1 mL was used for protein assays.

For the protein assays, 1 mL of a 0.1% triton lysis solution (in PBS) was added to each well to lyse the cells. 25 µL from each well was taken (in triplicate) and placed in two different 96 well plates to determine total protein content and alkaline phosphatase activity. A Pierce™ BCA

Protein assay was performed using provided protocol (Thermo Scientific) to determine total protein content. Samples in the BCA 96 well plate were incubated for 30 minutes with 200 µL of BCA solution. Absorbance readings were taken on an Infinite ® M200 (Tecan, Männedorf, Switzerland) at 562 nm. The alkaline phosphatase assay was performed using the ALP assay (Abcam ®). Samples in the ALP 96 well plate were incubated for 20 minutes with 100 µL of p-nitrophenol phosphate in assay buffer. Absorbance readings were taken on an Infinite ® M200 (Tecan, Männedorf, Switzerland) at 405 nm. Blank readings were subtracted from each data point of each assay and via the standard curve absorbance values were converted to total protein content and ALP activity for the BCA and ALP assays respectively.

3.5. qRT-PCR

2 mL aliquots were centrifuged at 200 g for 6 minutes. Supernatant was removed and aliquots were flash frozen in liquid nitrogen. Total RNA (250 ng) was isolated and reserve-transcribed to cDNA as previously described [27]. Primer sets directed against gene targets of interest were designed through National Center for Biotechnology Information's Primer-BLAST primer designing tool and synthesized at McMaster's Mobix Labs (Table 1). Quantitative analysis of mRNA expression was performed via qPCR using SsoAdvanced™ Universal SYBR® Green Supermix (BioRad) and CFX384 Touch Real-Time PCR Detection System (BioRad). The cycling conditions were 95°C for 10 min, followed by 40 cycles of 95°C for 10 secs and 60°C for 10 secs and 72°C for 15 secs. Relative fold changes were calculated using the comparative cycle times (Ct) method, normalizing all values to the geometric mean of three endogenous control genes (18S, ACTB, GAPDH). The endogenous control gene was selected based on experimentally-determined Ct stability across all treatment groups. Given that all primer sets had equal priming efficiency, the ΔCt values for each primer set were calibrated to the average of all

control Ct values, and the relative abundance of each primer set compared with calibrator was determined by the formula 2ΔΔCt, in which ΔΔCt was the normalized value.

**Table 1.** Forward and reverse sequences for the primers used for qPCR.

| Gene | Forward | Reverse | GenBank |
|---|---|---|---|
| ***18S (RNA18S 5)*** | CACGCCAGTACAAGATCCCA | AAGTGACGCAGCCCTCTATG | NR_003286.2 |
| ***ACTB*** | TTACAGGAAGTCCCTTGCCATC | GCAATGCTATCACCTCCCCTG | NM_001101.5 |
| ***GAPDH*** | TCACCATCTTCCAGGAGCGA | ATGACGAACATGGGGGCATC | NM_001357943.1 |
| ***ALPL*** | AGGACGCTGGGAAATCTGTG | CATGAGCTGGTAGGCGATGT | AH005272.2 |
| ***MMP9*** | CCGGCATTCAGGGAGACGCC | TGGAACCACGACGCCCTTGC | NM_004994.2 |
| ***TIMP1*** | GGGCTTCACCAAGACCTACA | TGCAGGGGATGGATAAACAG | NM_003254.3 |
| ***TIMP2*** | GAAGAGCCTGAACCACAGGT | GGGGGAGGAGATGTAGCAC | NM_003255.4 |

3.6. Scanning Electron Microscopy

Bioprinted samples were prepared and allowed to incubate for 1 day. Samples were then fixed with 0.25% glutaraldehyde in a sodium cacodylate buffer. Following this, the samples were stained with osmium tetraoxide before being sequentially dehydrated with ethanol starting at 25% (in Milli-Q water) to 100%. Samples were critically point dried (Leica Microsystems,

Wetzlar, Germany) and coated with 5 nm of platinum before being examined under SEM (TESCAN VP. SEM at 10kV). Samples were cut in half using a scalpel blade and imaged in cross-section.

### 3.7. Statistics

Statistical analysis for cell viability, protein assays, PCR and SEM image analysis was performed using the programming language, R (R Core Team, New Zealand). Protein assays used two-way ANOVA at a significance of $\alpha = 0.05$ and Tukey's HSD test was used to evaluate contrasts. All other methods were evaluated using the student's t-test with an accepted statistical significance of $p<0.05$.

## 4. Results

### 4.1. Mechanical testing

The mechanical properties of the samples were evaluated to determine the difference in Young's modulus between the 2L and 3H conditions using the initial linear region (Figure 2). Using Microsquisher testing machine, a platen was pressed against surface of the hydrogel and force applied to the platen and its displacement was measured. Figure 2 shows the stress vs. strain diagram for each of the samples. As expected, 3H samples had greater Young's modulus compared to 2L samples ($35.8 \pm 1.98$ MPa vs. $1.08 \pm 0.56$ MPa for 3H and 2L respectively).

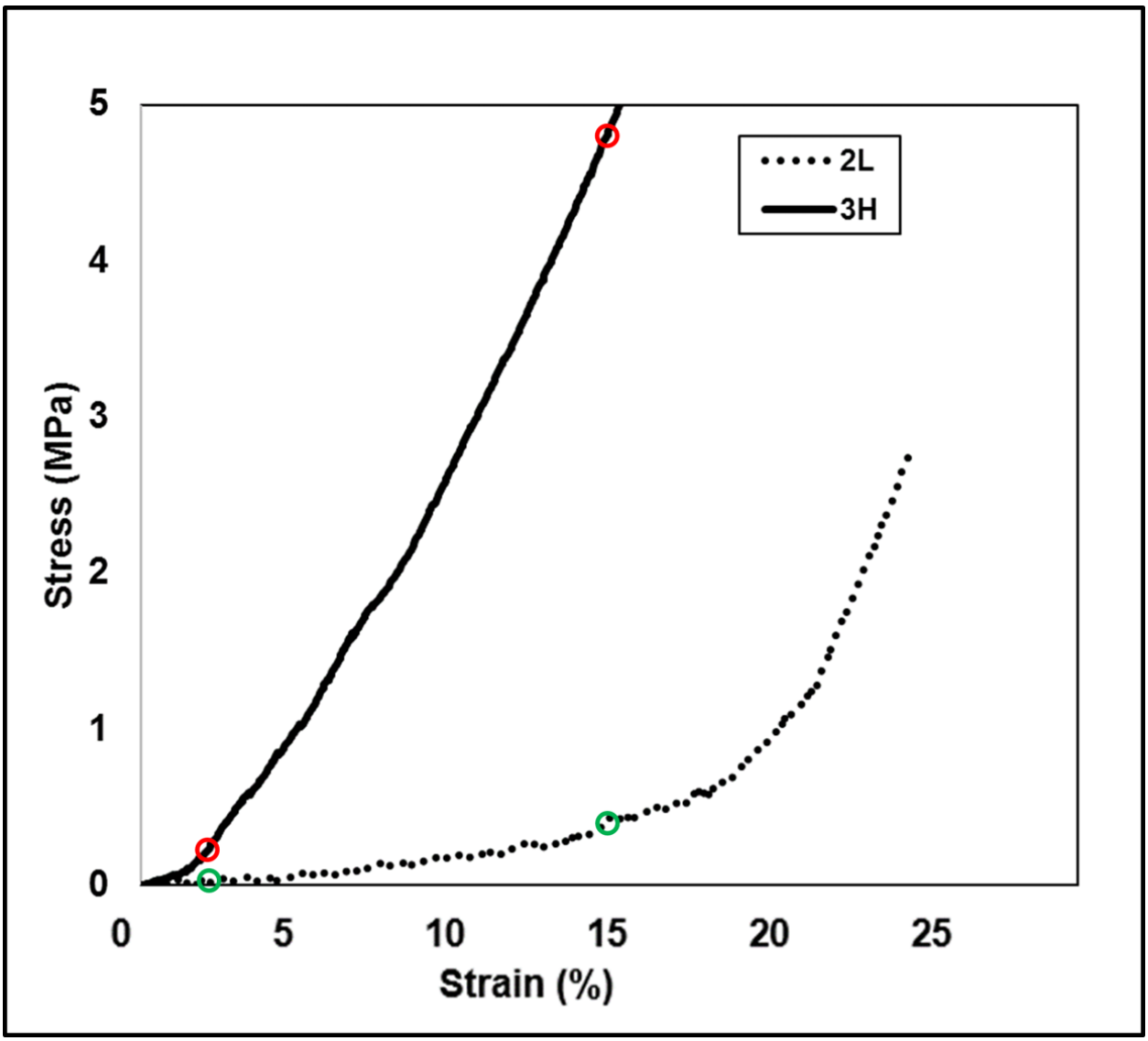


**Figure 2.** Stress vs. Strain diagram of 2L and 3H bioprinted samples demonstrating the improved mechanical properties of the 3H compared to 2L samples. The 2L and 3H samples both deform elastically with the 3H (35.8 MPa) being considerably stiffer ($p < 0.05$) than 2L (1.08) for 4 samples. The red circles indicate the start and end points for determining the modulus of the 3H samples while the green circles do the same for the 2L samples.

4.2. Viability

The viability of cells bioprinted within 2L and 3H hydrogels was evaluated using a live/dead stain kit after 1 day of incubation following printing (Figure 3). There were numerous live cells in both 2L and 3H samples, indicating that the printing process has a minimal effect on the cell viability. This is confirmed by Figure 3E which shows that there is no difference in the ratio of live to dead cells ($p<0.05$) between 2L and 3H samples. There is noticeable autofluorescence in the images which is a consequence of the printing process as the cellulose-based paper fluoresces significantly. As a control, cells were cultured on paper alone and evaluated in terms of cell metabolism after one day of incubation. The results indicate that there is no statistically significant change in metabolism between cells cultured on paper or traditional cell culture polystyrene ($p<0.05$) (Supplementary Figure 2). Cells embedded in the 2L and 3H samples were stained with Nile Red and DAPI and imaged under an upright microscope (Figure 4). The cells in the 3H samples were found to be statistically significantly smaller than the cells in the 2L samples ($p<0.05$ over 3 samples). The average diameter, with the cells being modelled as circles, for the 2L and 3H samples were 40.1 and 21.3 μm respectively. With 10 different focal planes being considered in the analysis for each sample, the cells in the 3H samples were found to be 70-80% smaller by area compared to the cells in the 2L samples.

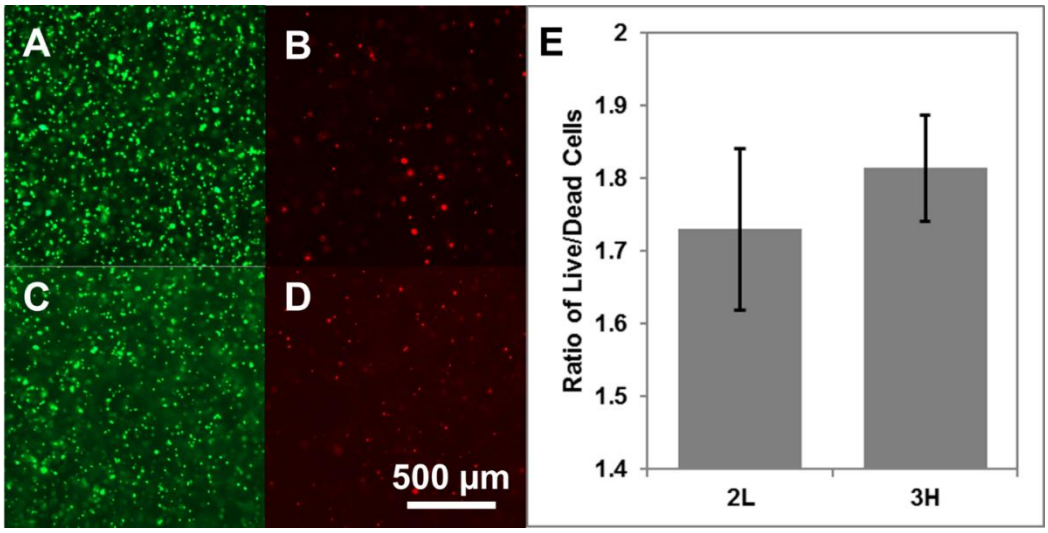


**Figure 3.** Live/dead stain fluorescent images taken for 2L (A/B) and 3H (C/D) after 1 day of incubation following bioprinting (n=3). Qualitatively, there are numerous live cells in both 2L and 3H samples and relatively few dead cells. The ratio of live to dead cells through fluorescent readings was determined to be statistically the same for 2L and 3H samples.

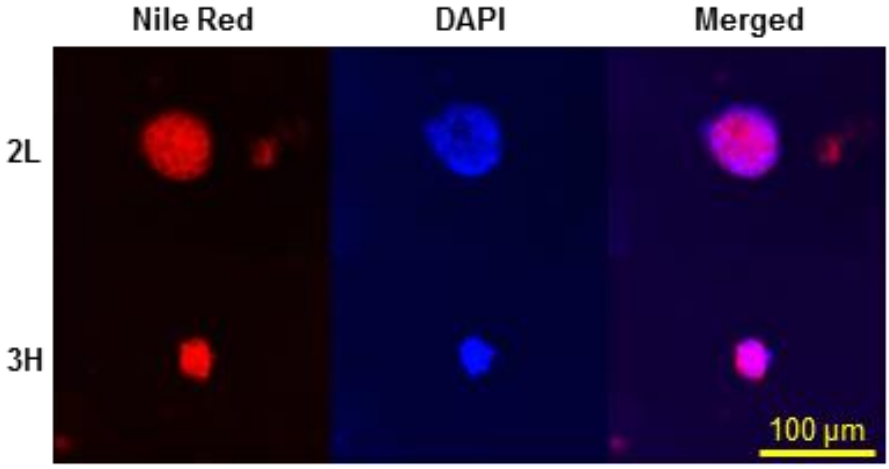


**Figure 4.** Nile Red and DAPI stained A) 2L and B) 3H samples. Saos-2 cells are multinucleated resulting in significant staining of membranes from both Nile Red and DAPI. Cells are visibly and quantifiably smaller in size (20.3 vs. 40.1 mm by diameter) in the 3H hydrogel compared to 2L hydrogel.

### 4.3. Protein Assays

2L and 3H samples with cells were evaluated *in vitro* for alkaline phosphatase (ALP) activity and total protein content (Figure 5). Over time, ALP activity showed statistically significant increases from 1 to 4 to 7 to 14 days for 2L ($p<0.05$). This effect was not observed for the 3H surface where ALP activity was statistically the same across all time points. When comparing between the groups, at the 4, 7 and 14 time points, the 3H samples showed statistically significantly less ALP activity compared to 2L samples ($p<0.05$). For total protein content, there were no significant differences between 2L and 3H sample groups. When normalizing ALP activity with respect to total protein content, the same statistical effects were observed as were seen in ALP activity alone. This provides additional evidence that comparable amounts of cells were successfully embedded, and viability was the same within the different printed hydrogel samples.

Confirmation that the embedding effect is influencing the change in ALP activity was achieved by comparing ALP activity and total protein content between cells embedded and cells simply cultured on paper for 4 days (Supplementary Figure 3). There was no statistically significant difference in ALP activity or total protein content between cells cultured only on the two different calcium treated papers ($p<0.05$).

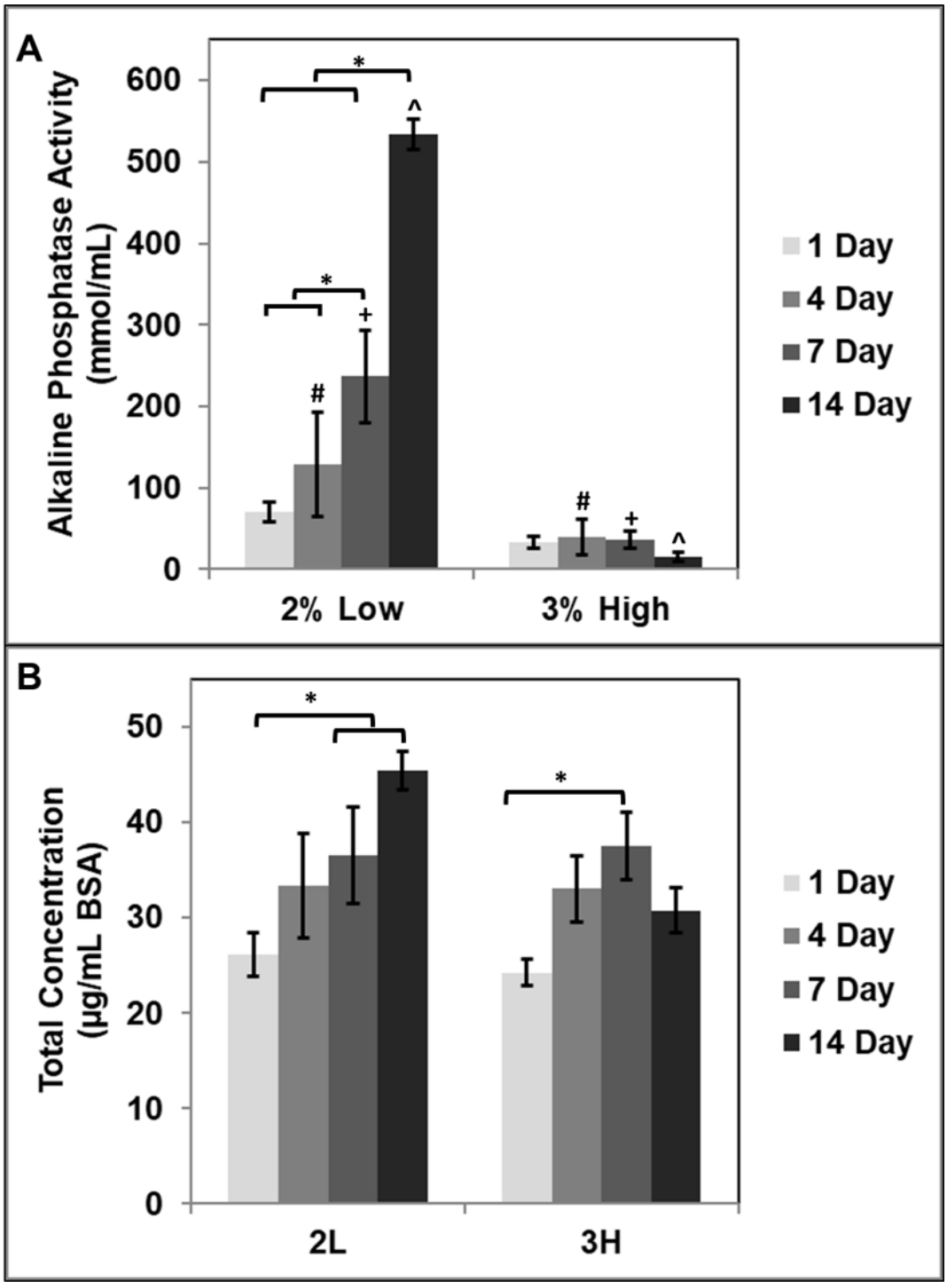


**Figure 5.** Alkaline phosphatase (ALP) activity, normalized by volume, (A) and total protein content (B) for 2L and 3H samples after 1, 4, 7 and 14 days of incubation (n = 5). ALP activity increases over time with 2L samples but remains statistically constant in 3H samples. ALP

activity was significantly less in 3H samples at 4, 7 and 14 time points ($p<0.05$). There are no statistically significant differences in total protein content between samples at each time point.

4.4. PCR

qRT-PCR was performed on 2L and 3H samples after 4 days of incubation. mRNA levels of ALPL, MMP9 and TIMP2 were significantly decreased in 3H samples compared to 2L samples ($p<0.05$; Figure 6A, B, D). mRNA levels of TIMP1 remained unchanged (Figure 6C).

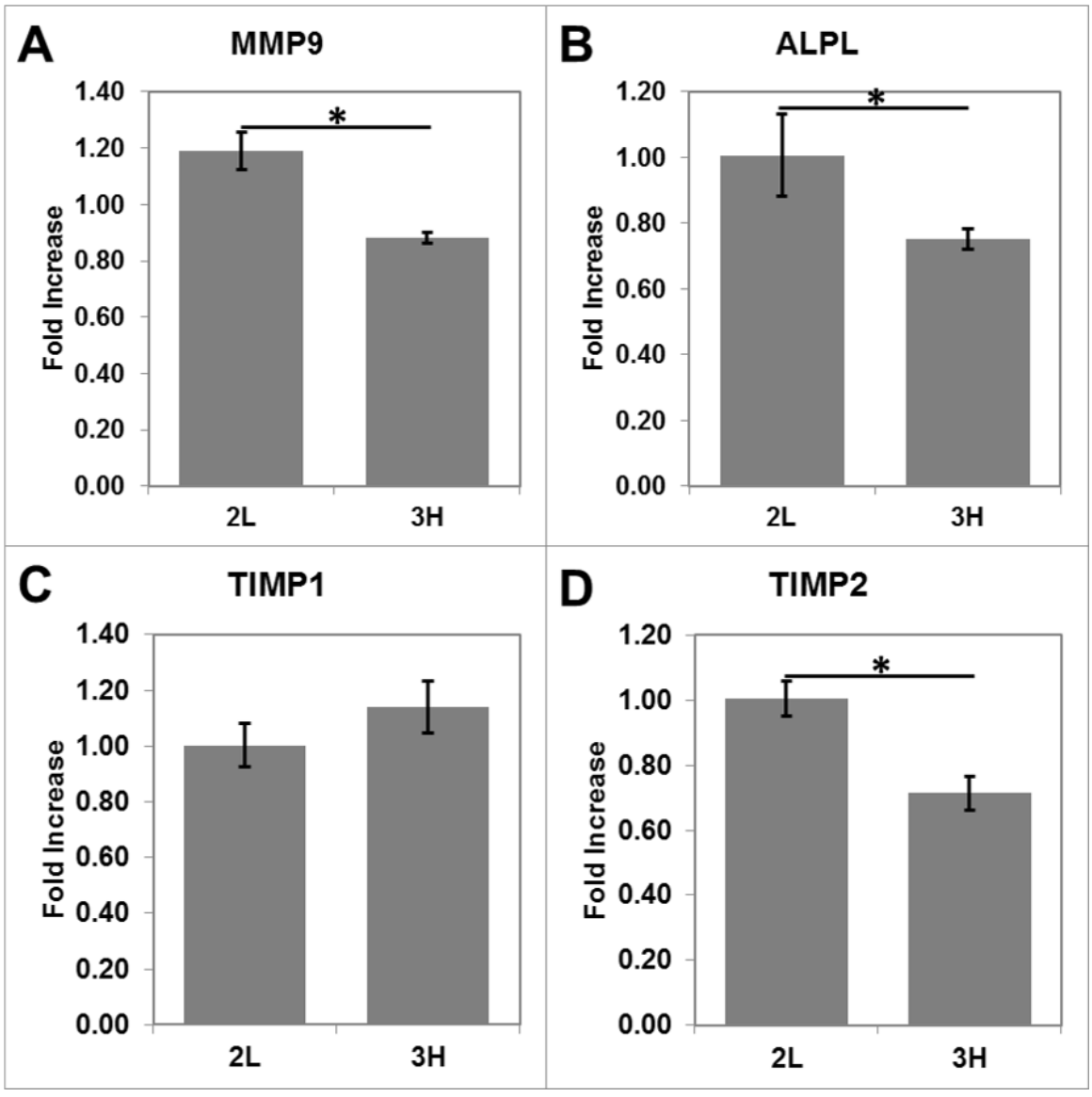

**Figure 6.** Normalized fold increases of (A) ALPL, (B) MMP9, (C) TIMP1 and (D) TIMP2 genes from qRT-PCR of 2L and 3H samples. There were statistically significant decreases ($p<0.05$, *) in expression of ALPL, MMP9 and TIMP2 genes in the 3H samples compared to 2L samples.

4.5. SEM

2L and 3H bioprinted samples were examined under SEM to observe how cells were embedded within the hydrogel matrix (Figure 7). Numerous cells can be identified in cross-section and top-down SEM images (Figures 7A, B). The cells appear as nodules on the surface and pores are not visible due to the hydrogel thickness being reduced during the dehydration steps required to image in SEM. The cells appear well distributed throughout the matrix and there are cellular processes that appear to extend within the hydrogel matrix (Figure 7C).

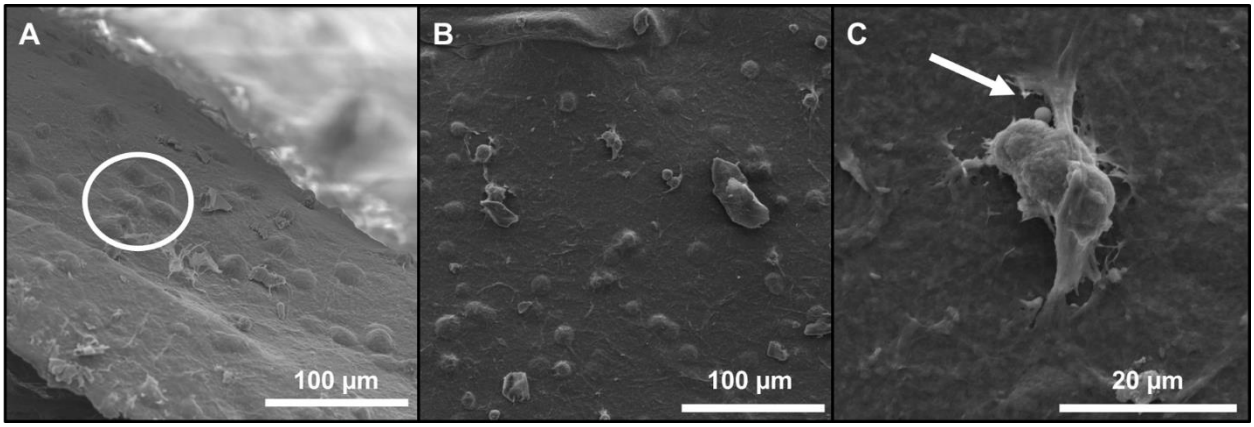


**Figure 7.** SEM images demonstrating how embedded cells are organized within the hydrogel matrix. Cells embedded (white circle) in 2L samples can be viewed in cross-section (A) and top-down (B) and are well-distributed. Cellular processes (white arrow) from the cells that extend into and within the matrix can also be observed (C).

## 5. Discussion

Osteoblast-like cells were successfully encapsulated in hydrogel using an ExCeL bioprinting setup to alter their phenotype to that similar to osteocytes. This change in phenotype was induced by differing hydrogel stiffness as a result of altering the amount of crosslinking agent and hydrogel solution. Two distinct hydrogels, 2L and 3H, were printed with notable differences in Young's modulus under compression. By increasing the stiffness of the matrix, it was hypothesized that osteoblasts would be entrapped and less capable of migration and that this system would encourage a change in phenotype from osteoblast to osteocyte.

The different printing conditions were determined to have no statistically significant effect on the viability of the cells. Other work has identified that materials with differing stiffness can effect cell function, viability and in some cases induce apoptosis [28], [29], however, this was not the case for the 2L and 3H hydrogels used in this work. It was further confirmed by SEM images which demonstrate that cells were distributed across the entirety of the hydrogel matrix with cellular processes extended within the matrix. In natural bone, these extended cellular processes enable osteocytes to communicate with other cells through the lacunar-canalicular network. As such, it is promising that these cellular processes have been preserved and that the osteogenic cells embedded in hydrogel are expressing an osteocyte-like phenotype.

The change in phenotype of osteoblast-like, Saos-2, cells towards that of osteocytes was confirmed via Nile red/DAPI staining, protein assays, and qRT-PCR. Fluorescent staining showed the cells were 70-80% smaller in 3H samples compared to 2L samples. This provides evidence that an osteocyte-like phenotype was induced as other work has shown that mature osteocytes are approximately 70% smaller than osteoblasts [30], [31]. Alkaline phosphatase (ALP) is an enzyme primarily produced at sites of bone growth and is considered a marker for

osteoblastic activity [32]. ALP is also typically not expressed, or weakly expressed, in osteocytes [16]. Protein assays demonstrated that ALP activity was significantly decreased for cells printed in the 3H hydrogels without any change in total protein content. This effect, both for ALP activity and total protein content, was observed over time up to 14 days suggesting that the cells maintain their altered phenotype in the designed system. qRT-PCR confirmed this change in expression as the ALPL gene was significantly down-regulated at the mRNA level for cells encapsulated in the 3H hydrogel. mRNA levels of MMP9 and TIMP2 were also significantly down-regulated in 3H samples, which suggests a reduction in cell migration [28], [29] and further supports that the Saos-2 cells are encapsulated by the hydrogel matrix. MMP9 and TIMP2 are known to be markers of bone remodeling [33], [34], [26], as increased expression of both genes have been observed at sites of bone remodeling or high osteoblastic activity [33], [34]. Mouse in vivo studies conducted by others indicate that TIMP2 may inhibit osteoblastic differentiation into osteocytes [35], while emphasizing the importance of the MMP family for proper transformation of osteoblasts into osteocytes [36]. These studies are in agreement with the decreased TIMP2 expression observed in 3H samples compared to 2L samples. Similarly, the balance of expression between the two is important as an imbalance of MMP to TIMP genes has been suggested to lead to bone loss [34].These changes in expression, at the protein and gene level, indicate that the different mechanical properties between the 2L and 3H hydrogel are capable of inducing osteoblast-like to osteocyte-like differentiation.

This work used Saos-2 cells, an immortalized cell line considered a good model for osteoblast activity [32]. These cells are generally considered incapable of differentiating into other types of cells, osteocytes included [32], and as such, this work represents the first step towards the development of a model for osteocyte differentiation. Future iterations would require either bone

mesenchymal stem cells or primary human osteoblasts to identify how the phenotype of these cells could be adjusted by modulating the mechanical properties of the printed hydrogels. Mesenchymal stem cells could be differentiated into osteoblasts using known methods, such as dexamethasone treatment, and subsequently encapsulated in the process described in this work [37]. The modulus of the scaffolds, while noticeable different from each other, does not approach the known modulus of bone which is typically estimated to be between 7-30 GPa [38]. The current scaffolds do not have any mineral present beyond what is produced by the cells, so future work could see the addition of hydroxyapatite to simulate the mineral presence in bone and subsequently stiffen the material [16]. Additionally, a more physiologically relevant model could be constructed using a co-culture system to characterize the interactions between the various cell types present during bone remodeling.

## 6. Conclusion

An *in vitro* model to study osteoblast entrapment was created using a paper-based bioprinting technique. By altering the amount of crosslinking in an alginate hydrogel, two gels with drastically different Young's moduli were generated. When osteoblast-like cells were bioprinted, the stiffer gels resulted in smaller cells without any decrease in overall cell viability. The alkaline phosphatase activity was greatly reduced in the stiffer hydrogel while the total protein content remained the same. Similarly, expression levels of osteoblast relevant genes were all reduced in the stiffer hydrogel, which along with the reduced size and protein expression demonstrates that an osteocyte-like behavior has been induced. This *in vitro* model is a stepping stone towards larger studies of osteocyte-osteoblast behavior that could be explored by interfacing this *in vitro*

model with mechanical stimuli, or by using it as a platform for drug discovery, or biomaterials testing to observe complex bone cell behavior.

## ASSOCIATED CONTENT

**Supplementary Figure 1.** Alkaline phosphatase activity for 2L, 2H, 3L, and 3H bioprinted samples. 2L and 3H conditions were chosen for further examination as the 2H and 3L ALP activity was statistically equivalent.

**Supplementary Figure 2.** Cell metabolism readings for Saos-2 cells grown on the calcium treated paper alone, without any hydrogel encapsulation. Data shows that there was no statistically significant difference in cell metabolism between samples.

**Supplementary Figure 3.** Alkaline phosphatase activity (A) and total protein content (B) of 2L and 3H samples both grown on calcium-treated paper (red) and bioprinted (blue). The ALP activity for bioprinted 3H samples is statistically significantly lower compared to bioprinted 2L samples while total protein content remains statistically the same. There is no significant difference in ALP activity or total protein content for the sample cultured on the paper alone.

**Supplementary Figure 4.** Alkaline phosphatase (ALP) activity (A) and total protein content (B) for 2L and 3H samples after 7 and 14 days of incubation.

## AUTHOR INFORMATION

### Corresponding Author

*To whom correspondence should be addressed:

Email: kgrandfield@mcmaster.ca, selvaga@mcmaster.ca

**Present Addresses**

†If an author's address is different than the one given in the affiliation line, this information may be included here.

**Author Contributions**

The manuscript was written through contributions of all authors. All authors have given approval to the final version of the manuscript. ‡B.E.J. L and A.S contributed equally.

**Funding Sources**

We would like to acknowledge the support of the Natural Sciences and Engineering Research Council of Canada (NSERC) and the Discovery Grant Program (RGPIN 2014-06053). PRS acknowledges support from the Canada Research Chairs Program and the NSERC Discovery Accelerator Supplement.

ACKNOWLEDGMENTS

We would like to acknowledge the support of the Natural Sciences and Engineering Research Council of Canada (NSERC) and the Discovery Grant Program (RGPIN 2014-06053). PRS acknowledges support from the Canada Research Chairs Program and the NSERC Discovery Accelerator Supplement. Microscopy was carried out at the Faculty of Health Sciences Electron Microscopy Facility at McMaster University. *In vitro* studies were performed at the Biointerfaces Institute at McMaster University.

ABBREVIATIONS

2L; 2 wt% alginate in McCoy's media with low calcium concentration, 3H; 3 wt% alginate in McCoy's media with high calcium concentration, Ca; calcium, ALP; alkaline phosphatase, ExCeL; Combining extrusion printing on cellulose scaffods with lamination, mRNA; messenger

ribonucleic acid, MMP9; matrix metallopeptidase 9, TIMP1; tissue inhibitor of metalloproteinase 1, TIMP2; tissue inhibitor of metalloproteinase 2, ALPL; alkaline phosphatase, GAPDH; Glyceraldehyde 3-phosphate dehydrogenase, ACTB; beta-actin, 2D; 2 dimensional, 3D; 3 dimensional, ECM; extracellular matrix, ABA; alamar blue assay, BCA; bicinchoninic acid, qRT-PCR; quantitative reverse transcription polymerase chain reaction, SEM; scanning electron microscopy, DAPI; 4′,6-diamidino-2-phenylindole, PBS; phosphate buffered saline, FBS; fetal bovine serum, ANOVA; analysis of variance, Tukey's HSD; tukey's honest significant difference.

## REFERENCES


[1] T. A. Franz-Odendaal, B. K. Hall, and P. E. Witten, "Buried alive: How osteoblasts become osteocytes," *Dev. Dyn.*, vol. 235, no. 1, pp. 176–190, 2006.

[2] S. L. Dallas and L. F. Bonewald, "Dynamics of the transition from osteoblast to osteocyte," *Ann. N. Y. Acad. Sci.*, vol. 1192, pp. 437–443, 2010.

[3] F. Paic *et al.*, "Identification of differentially expressed genes between osteoblasts and osteocytes," *Bone*, vol. 45, no. 4, pp. 682–692, 2009.

[4] M. Capulli, R. Paone, and N. Rucci, "Osteoblast and osteocyte : Games without frontiers," *Arch. Biochem. Biophys.*, vol. 561, pp. 3–12, 2014.

[5] R. Civitelli, "Cell-cell communication in the osteoblast/osteocyte lineage," *Arch. Biochem. Biophys.*, vol. 473, no. 2, pp. 188–192, 2008.

[6] K. Duval *et al.*, "Modeling Physiological Events in 2D vs. 3D Cell Culture," *Physiology*, vol. 32, no. 4, pp. 266–277, 2017.

[7] B. M. Baker and C. S. Chen, "Deconstructing the third dimension – how 3D culture microenvironments alter cellular cues," *J. Cell Sci.*, vol. 125, no. 13, pp. 3015–3024, 2012.

[8] D. Anton, H. Burckel, E. Josset, and G. Noel, "Three-dimensional cell culture: A breakthrough in vivo," *Int. J. Mol. Sci.*, vol. 16, no. 3, pp. 5517–5527, 2015.

[9] C. M. Nelson, J. L. Inman, and M. J. Bissell, "Three-dimensional lithographically defined organotypic tissue arrays for quantitative analysis of morphogenesis and neoplastic progression," *Nat. Protoc.*, vol. 3, no. 4, pp. 674–678, 2008.

[10] A. Abbott, “Cell culture: biology’s new dimension,” vol. 424, no. August, 2003.
[11] A. Wodarz and I. Näthke, “Cell polarity in development and cancer,” *Nat. Cell Biol.*, vol. 9, no. 9, pp. 1016–1024, 2007.
[12] S. J. Morrison and J. Kimble, “Asymmetric and symmetric stem-cell divisions in development and cancer,” *Nature*, vol. 441, no. 7097, pp. 1068–1074, 2006.
[13] F. Coşkun and C. R. Parks, “A molecular phylogeny of Cercis L. (fabaceae) using the chloroplast trnl-F DNA sequences,” *Pakistan J. Bot.*, vol. 41, no. 4, pp. 1587–1592, 2009.
[14] Y. Kato, J. J. Windle, B. A. Koop, G. R. Mundy, and L. F. Bonewald, “Establishment of an Osteocyte-like Cell Line, MLO-Y4,” *J. Bone Miner. Res.*, vol. 12, no. 12, pp. 2014–2023, 2010.
[15] D. Nicolella, V. Dusevich, M. R. Dallas, J. D. Eick, and L. F. Bonewald, “Mechanism by which MLO-A5 Late Osteoblasts / Early Osteocytes Mineralize in Culture : Similarities with Mineralization of Lamellar Bone,” pp. 340–353, 2006.
[16] F. Boukhechba *et al.*, “Human primary osteocyte differentiation in a 3D culture system,” *J. Bone Miner. Res.*, vol. 24, no. 11, pp. 1927–1935, 2009.
[17] K. Uchihashi, S. Aoki, A. Matsunobu, and S. Toda, “Osteoblast migration into type I collagen gel and differentiation to osteocyte-like cells within a self-produced mineralized matrix : A novel system for analyzing differentiation from osteoblast to osteocyte,” *Bone*, vol. 52, no. 1, pp. 102–110, 2013.
[18] I. T. Ozbolat, W. Peng, and V. Ozbolat, “Application areas of 3D bioprinting,” *Drug Discov. Today*, vol. 21, no. 8, pp. 1257–1271, 2016.
[19] W. Peng, D. Unutmaz, and I. T. Ozbolat, “Bioprinting towards Physiologically Relevant Tissue Models for Pharmaceutics,” *Trends Biotechnol.*, vol. 34, no. 9, pp. 722–732, 2016.
[20] G. Gao, Y. Huang, A. F. Schilling, K. Hubbell, and X. Cui, “Organ Bioprinting: Are We There Yet?,” *Adv. Healthc. Mater.*, vol. 7, no. 1, pp. 1–8, 2018.
[21] Y. S. Zhang, *Three-Dimensional Bioprinting Strategies for Tissue Engineering*. Cold Spring Harbor Perspectives, 2017.
[22] S. Noh, *3D Bioprinting for Tissue Engineering*. Springer Singapore, 2018.
[23] H. W. Kang, S. J. Lee, I. K. Ko, C. Kengla, J. J. Yoo, and A. Atala, “A 3D bioprinting system to produce human-scale tissue constructs with structural integrity,” *Nat. Biotechnol.*, vol. 34, no. 3, pp. 312–319, 2016.
[24] J. Jang, H. G. Yi, and D. W. Cho, “3D Printed Tissue Models: Present and Future,” *ACS Biomater. Sci. Eng.*, vol. 2, no. 10, pp. 1722–1731, 2016.
[25] A. Shahin-Shamsabadi and P. R. Selvaganapathy, “ExCel: Combing Extrusion printing on Cellulose scaffolds with Lamination to create in vitro biological models,” *Biofabrication*, vol. 11, no. 3, 2019.
[26] E. Kostovski, N. Hjeltnes, E. F. Eriksen, S. O. Kolset, and P. O. Iversen, “Differences in Bone Mineral Density , Markers of Bone Turnover and Extracellular Matrix and Daily Life Muscular Activity Among Patients with Recent Motor-Incomplete Versus Motor-Complete Spinal Cord Injury,” *Calcif. Tissue Int.*, vol. 96, no. 2, pp. 145–154, 2015.
[27] M. K. Wong *et al.*, “Extracellular matrix surface regulates self- assembly of three-dimensional placental trophoblast spheroids,” pp. 1–18, 2018.
[28] J. D. Hood and D. A. Cheresh, “Role of integrins in cell invasion and migration,” *Nat. Rev. Cancer*, vol. 2, no. 2, pp. 91–100, 2002.
[29] G. Murphy and J. Gavrilovic, “Proteolysis and cell migration: Creating a path?,” *Curr. Opin. Cell Biol.*, vol. 11, no. 5, pp. 614–621, 1999.

[30] C. Palumbo, “A three-dimensional ultrastructural study of osteoid-osteocytes in the tibia of chick embryos,” *Cell Tissue Res.*, vol. 246, no. 1, pp. 125–131, 1986.
[31] Y. Sugawara, H. Kamioka, T. Honjo, K. I. Tezuka, and T. Takano-Yamamoto, “Three-dimensional reconstruction of chick calvarial osteocytes and their cell processes using confocal microscopy,” *Bone*, vol. 36, no. 5, pp. 877–883, 2005.
[32] C. Pautke *et al.*, “Characterization of Osteosarcoma Cell Lines MG-63 , Saos-2 and U-2 OS in Comparison to Human Osteoblasts,” *Anticancer Res.*, vol. 24, no. 6, pp. 3743–3748, 2004.
[33] G. Dew *et al.*, “Localisation of matrix metalloproteinases and TIMP-2 in resorbing mouse bone,” *Cell Tissue Res.*, vol. 299, no. 3, pp. 385–394, 2000.
[34] P. A. Hill and J. J. Reynolds, “Inhibition of stimulated bone resorption in vitro by TIMP-1 and TIMP-2,” *Biochim. Biophys. Acta (BBA)-Molecular Cell Res.*, vol. 1177, no. 1, pp. 71–74, 1993.
[35] M. A. Karsdal, T. A. Andersen, L. Bonewald, and C. Christiansen, “Matrix Metalloproteinases (MMPs) Safeguard Osteoblasts from Apoptosis during Transdifferentiation into Osteocytes: MT1-MMP Maintains Osteocyte Viability,” *DNA Cell Biol.*, vol. 23, no. 3, pp. 155–165, 2004.
[36] K. Holmbeck *et al.*, “MT1-MMP-Deficient Mice Develop Dwarfism, Osteopenia, Arthritis, and Connective Tissue Disease due to Inadequate Collagen Turnover MMP Unit cellular tools in embryonic development, in growth, in mammary involution, and in a number of diseases such,” *Cell*, vol. 99, pp. 81–92, 1999.
[37] A. Khojasteh *et al.*, “The Effect of Deproteinized Bovine Bone Mineral on Saos-2 Cell Proliferation,” *Iran. Endod. J.*, vol. 8, no. 3, pp. 118–122, 2013.
[38] Q. Chen, C. Zhu, and G. A. Thouas, “Progress and challenges in biomaterials used for bone tissue engineering : bioactive glasses and elastomeric composites,” *Prog. Biomater.*, vol. 1, no. 2, pp. 1–22, 2012.
[39] E. Axpe and M. L. Oyen, “Applications of Alginate-Based Bioinks in 3D Bioprinting,” *Int. J. Mol. Sci.*, vol. 17, no. 12, 2016.
[40] Q. Feng *et al.*, “Engineering a morphogenetically active hydrogel for bioprinting of bioarti fi cial tissue derived from human osteoblast-like SaOS-2 cells,” *Biomaterials*, vol. 35, pp. 8810–8819, 2014.